Materials Science in Semiconductor Processing 39 (2015) 649–653

Contents lists available at ScienceDirect

Materials Science in Semiconductor Processing

journal homepage: www.elsevier.com/locate/mssp

Source/drain metallization effects on the specific contact resistance of indium tin zinc oxide thin film transistors

Cam Phu Thi Nguyen, Thanh Thuy Trinh, Jayapal Raja, Anh Huy Tuan Le, Youn-Jung Lee, Vinh Ai Dao *, Junsin Yi *

Information and Communication Device Laboratory, School of Information and Communication Engineering, Sungkyunkwan University, Suwon 440-746, Republic of Korea

ARTICLE INFO

Available online 24 June 2015

Keywords:
ITZO-based TFT
S/D electrodes
Specific contact resistance
TLM mask

ABSTRACT

We report on the specific contact resistance of interfaces between thin amorphous semiconductor Indium Tin Zinc Oxide (ITZO) channel layers and different source/drain (S/D) electrodes (Al, ITO, and Ni) in amorphous oxide thin film transistors (TFTs) at different channel lengths using a transmission line model. All the contacts showed linear current–voltage characteristics. The effects of different channel lengths (200–800 μm, step 200 μm) and the contact resistance on the performance of TFT devices are discussed in this work. The Al/ITZO TFT samples with the channel length of 200 μm showed metallic behavior with a linear drain current-gate voltage (I_D–V_G) curve due to the formation of a conducting channel layer. The specific contact resistance (ρ_C) at the source or drain contact decreases as the gate voltage is increased from 0 to 10 V. The devices fabricated with Ni S/D electrodes show the best TFT characteristics such as highest field effect mobility (16.09 $cm^2/V\cdot s$), ON/OFF current ratio (3.27×10^6), lowest sub-threshold slope (0.10 V/dec) and specific contact resistance (8.62 $\Omega\cdot cm^2$ at V_G=0 V). This is found that the interfacial reaction between Al and a-ITZO semiconducting layer lead to the negative shift of threshold voltage. There is a trend that the specific contact resistance decreases with increasing the work function of S/D electrode. This result can be partially ascribed to better band alignment in the Ni/ITZO interface due to the work function of Ni (5.04–5.35 eV) and ITZO (5.00–6.10 eV) being somewhat similar.

1. Introduction

Recently, thin film transistors (TFTs) based on amorphous oxide semiconductors (AOSs) have been used for electronic applications, such as touch panels, active-matrix flat panel displays, and active-matrix organic light-emitting diode (AMOLED) displays, due to the improvement when compared with conventional amorphous and polycrystalline silicon based devices [1–3]. In particular, amorphous indium tin zinc oxide (a-ITZO) is a promising AOS candidate material with high mobility (>10 $cm^2/V\cdot s$) [4], high transparency ($>85\%$) in the visible range [5], and good uniform surface planarity [6] even the film is deposited at room temperature.

Specific contact resistance (ρ_C) is defined as the resistance presented to uniform current flow across the interface of unit area between the metallization and semiconductor layers. However, the contact properties between source/drain (S/D) electrodes and the a-ITZO channel layer at different channel lengths have not been reported. The accurate understanding

* Corresponding authors. Tel.: +82 31 290 7139; fax: +82 31 290 7159.
E-mail addresses: daovinhai@skku.edu (V.A. Dao), yi@yurim.skku.ac.kr (J. Yi).

http://dx.doi.org/10.1016/j.mssp.2015.05.069
1369-8001/

of these properties is important, because a high contact resistance in S/D contacts is the major cause of current crowding, wherein accumulated electron flows directly impact the electrical properties of TFTs, such as threshold voltage (V_{TH}), field effect mobility (μ_{FE}), ON/OFF current ratio (I_{ON}/I_{OFF}), and subthreshold swing (SS).

The a-ITZO is a natural n-type semiconductor. This is observed that In-5s and Sn-5s meet the electronic configuration $(n-1)d^{10}ns^{0}$ ($n \geq 5$) of heavy post-transition metal cation for AOS [3]. The conduction band minimum states of a-ITZO are found to consist mainly of the In-5s and Sn-5s atomic orbital states [7]. The In-5s and Sn-5s cations make similar contributions to form the electron conduction in the a-ITZO. Thus, the electron is the dominant carrier in the ITZO bulk. As Sunghwan Lee et al. [8] reported, the low carrier concentration in the TFT channel improve the performance of transistors. The improved specific contact resistance was acquired with a high carrier density which is not suitable for TFT channel material. Otherwise, when the contact resistance is large, a high applied bias is needed across the S/D to inject carriers into the device, resulting in low reported mobility. Furthermore, due to the high work function (4.9–6.1 eV) [9], and high carrier concentration of a-ITZO film, this is significant to find the S/D material to create low ρ_C on the contact between S/D electrodes and active layer.

The investigation described in this manuscript focuses on the influence of ρ_C on the interface between a-ITZO channel layer and S/D electrodes, and their effects on electrical characteristics of a-ITZO based TFTs to provide better performance. The degradation in the TFT performance of short channel structures owing to the contact resistance is also discussed. These resistances were extracted by the well-known transmission line method (TLM) with different channel lengths and gate voltages (V_G) applied.

2. Experimental

Fig. 1(a) shows the schematic cross-section view of the staggered bottom-gate structure ITZO–TFT. Commercially available SiO_2 coated *p*-type-crystalline silicon substrates (SiO_2 acting as the common gate insulator) were placed. These substrates were cleaned with acetone, iso-propyl-alcohol and de-ionized water in an ultrasonic bath for 10 min. The ITZO active channel was 50 nm thick and deposited by DC magnetron sputtering using a ceramic ITZO target (In_2O_3: SnO_2: ZnO = 30:35:35 at. %) at room temperature. The DC power and working pressure were maintained at 80 W and 5 m Torr, respectively. The ratio of Ar and O_2 gas flow rates were $Ar/O_2 = 14/6$. After the deposition, the samples were annealed using rapid thermal annealing (RTA) equipment at 350 °C for one hour under oxygen ambience in the furnace. The S/D electrodes were formed with 150 nm thickness. Al and Ni electrodes were deposited by thermal evaporation. The ITO electrode was deposited by DC sputtering system at 100 W, and 5 m Torr. For the investigation of specific contact resistance, TLM patterns consisting of a fixed channel width (W) of 1600 μm and lengths (L) ranging from 200 (short channel) to 800 μm (long channel) at 200 μm steps were formed in the same channel region (Fig. 1(a)). So the W/L ratios were 8/1, 4/1, 8/3, and 2/1, respectively. These structures offer a range of channel lengths to allow the extraction of channel resistivity and channel/metallization specific contact resistance via the TLM method [8,10]. The electrical performance of the TFT devices was characterized using an EL 420 C semiconductor parameter analyzer. All the measurements were carried out at room temperature in the dark.

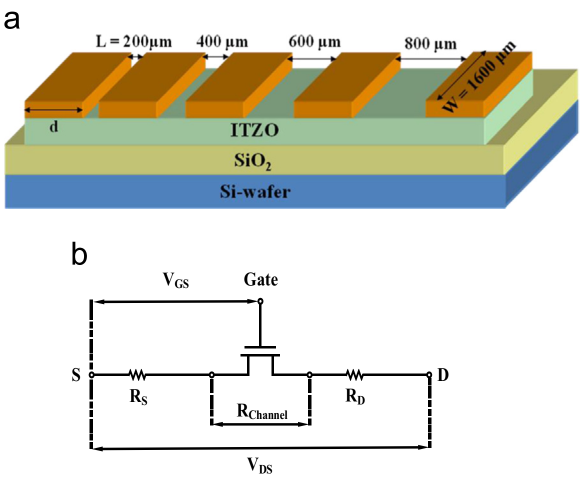

Fig. 1. (a) Schematic diagram of TLM patterns in ITZO TFTs and (b) an equivalent circuit model for TFTs.

3. Results and discussions

Fig. 1(b) shows the schematic diagram of TLM patterns in ITZO TFTs. The total resistance (R_{Total}) measured in each of the TLM configurations is a function of the contact resistance at the two channel/contact interfaces and the sheet resistance of the channel [8,11]:

$$R_{Total} = 2R_C + R_{ch} \tag{1}$$

with

$$R_{ch} = \frac{R_S}{W} L \tag{2}$$

where R_C is the contact resistance between channel and S/D electrodes, R_S is the sheet resistance of the semiconducting layer outside the contact, and R_{ch} is the channel resistance.

The relationship between contact resistance R_C and ρ_C is given by [10]

$$R_C = \frac{1}{W}\sqrt{R_S \rho_C}\coth\left(\sqrt{\frac{R_S}{\rho_C}}d\right) \approx \frac{1}{W}\sqrt{R_S\rho_C} \approx \frac{\rho_C}{WL_T} \tag{3}$$

$$L_T = \left(\frac{\rho_C}{R_S}\right)^{1/2} \tag{4}$$

where d is the contact length and L_T is the transfer length, which is the effective length of the S/D electrodes.

Fig. 2 presents the transfer characteristics of ITZO–TFTs with Al S/D contacts at drain voltage $V_D = 1$ V. The V_G is swept from −15 to 15 V. The threshold voltage of the TFTs increases with increasing L. The samples with the W/L

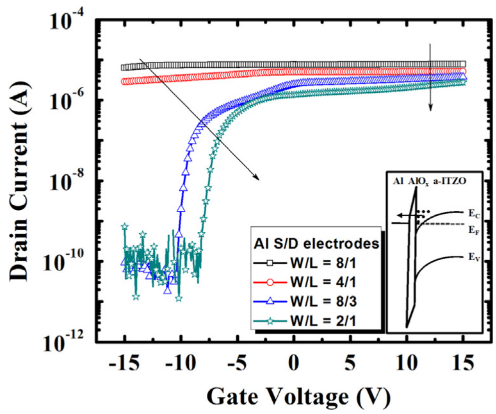

Fig. 2. Transfer characteristics of ITZO–TFTs with Al S/D contacts at $V_D=1$ V at varying channel lengths. Inset: energy band diagram of Al/ITZO TFT.

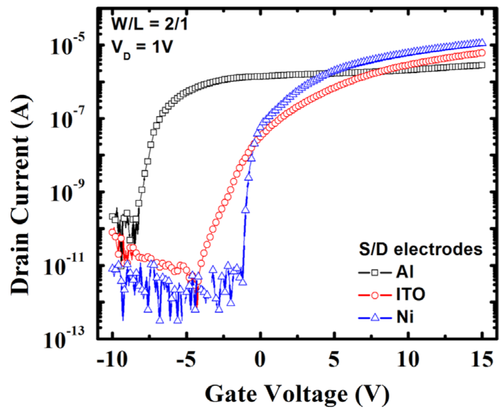

Fig. 3. Transfer characteristics (at $V_D=1$ V) of ITZO–TFTs with different S/D contacts.

ratio of 8/1 and 4/1 show the metallic behavior with an almost linear I_D–V_G curve due to the formation of a conducting channel layer. This behavior may be explained by the formation of thin aluminum oxide (AlO_x) at the Al/ITZO interface. The formation enthalpy of Al_2O_3 ($\Delta H_{Al_2O_3}=-1675.7$ kJ/mol) is lower than that of In_2O ($\Delta H_{In_2O}=-167$ kJ/mol), In_2O_3 ($\Delta H_{In_2O_3}=-926$ kJ/mol), SnO ($\Delta H_{SnO}=-280.7$ kJ/mol), SnO_2 ($\Delta H_{SnO_2}=-577.6$ kJ/mol), and ZnO ($\Delta H_{ZnO}=-350.5$ kJ/mol) [12]. So the formation of AlO_x at the interfacial region between Al and ITZO layers by oxygen out-diffusion from ITZO is reasonable [13,14]. As shown in the inset of Fig. 2, we assume that these thin non-stoichiometric layers AlO_x will generate barrier height at the interface to prevent electron transportation. In general, negative V_{TH} shifts for n-type TFTs are believed to be associated with the relatively large carrier concentration of ITZO. In this experiment, ITZO layer thickness and process conditions were identically confined. The formation of AlO_x interfacial layer retains oxygen vacancies at the surface of the ITZO channel layer. Therefore, the negative shift in V_{TH} in Al/ITZO case can be interpreted as an increased carrier concentration in the ITZO semiconducting layer after interfacial reactions. Otherwise, near the junctions, carriers diffuse to the channel from a higher concentration to a lower concentration [15]. The effect of these carriers becomes stronger as L is shorter and consequently a negative V_{TH} shift. This may change the overall carrier concentration of the channel region. At the short channel devices, the number of electron increase rapidly in the short time by tunneling throughout the thin AlO_x layer. Hence, the carrier concentration increases too fast in the channel region and then V_{TH} shifts to negative side. However, for long channel devices, the change of overall carrier concentration in the channel become slowly due to the long distance between S and D contacts. Note that the same density of states (DOS) can be assumed for both long-channel and short-channel TFTs because they were all fabricated under the same process conditions. However, the reduction on the carrier density of the S/D regions increases the contact resistance, resulting in a reduction in ON current (I_{ON}). Therefore, tradeoffs between lower I_{ON} and less V_{TH} dependence on L have to be considered.

Table 1
The electrical parameters of ITZO-based TFT devices using varying S/D electrodes.

TFT parameters	Source/Drain electrodes		
	Al	ITO	Ni
V_{TH} (V)	−3.96	0.58	4.24
V_{ON} (V)	−8.28	−4.28	−1.18
SS (V/dec)	0.49	0.82	0.10
μ_{FE} cm^2/V·s)	3.94	10.34	16.09
I_{ON}/I_{OFF}	3.97×10^4	9.63×10^5	3.27×10^6

Fig. 3 presents the transfer characteristics of ITZO–TFTs with different S/D contacts with the W/L ratio of 2/1 at $V_D=1$ V. The turn-on voltage (V_{ON}) and V_{TH} are shifted to the positive side for Ni electrodes. The TFT electrical characteristics, such as μ_{FE}, V_{ON}, V_{TH}, SS, and I_{ON}/I_{OFF} with different S/D contacts are shown in Table 1. TFTs with Al electrodes show the depletion mode with $V_{TH}=-3.96$ V, $\mu_{FE}=3.94$ cm^2/V·s, SS$=0.49$ V/dec, and $I_{ON}/I_{OFF}=3.97\times10^4$. The TFT devices with ITO and Ni electrodes show the operation of enhanced modes. The TFT with the Ni electrodes has $V_{TH}=4.24$ V, $\mu_{FE}=16.09$ cm^2/V·s, $SS=0.10$ V/dec, and $I_{ON}/I_{OFF}=3.27\times10^6$. The higher μ_{FE} leads to higher TFT switching speed and therefore Ni/ITZO device shows higher on current. The better performance of TFTs realized by employing electrode materials such as ITO, and Ni may be due to the smaller ρ_C compared to the devices using Al S/D electrodes.

The I–V characteristics of contact behavior at the interface of ITZO channel and S/D electrodes at the bias range from −5 to +5 V is shown in Fig. 4. For I–V measurement, an ITZO film 50 nm-thick was deposited on a glass substrate (Corning Eagle XG) using a TLM mask. It was observed that all contacts showed a linear I–V curve indicating that the ohmic contacts were formed with all used electrodes. This means that the work functions (Φ) of Al, ITO, and Ni are lower than ITZO [16,17].

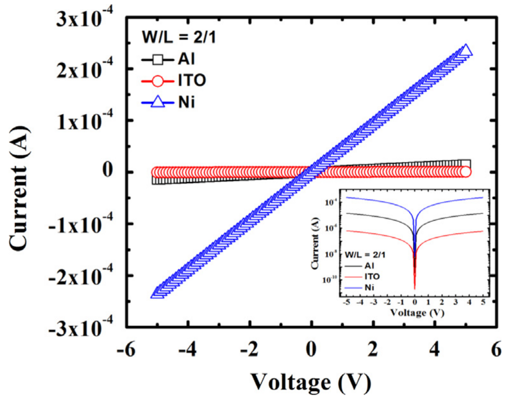

Fig. 4. *I–V* characteristics of ITZO active channel and Al, ITO, and Ni electrodes.

The effect of V_G on the interfacial contact resistance in the TFT/TLM structures was found by repeating the TLM measurements at V_G from 0 to 10 V in 2 V steps; the resulting families of R_{Total} versus d curves (one per gate voltage) are plotted in Fig. 5. The intercept and slope of each line in Fig. 5 was used to find R_C and R_{ch}, respectively. The positive V_G modulates ρ_C. As shown in Fig. 6(a), the TFT devices using Ni S/D electrodes has the lowest ρ_C. Converting R_C to ρ_C via Eqs. (3) and (4) for each gate voltage yields the ρ_C versus V_G result plotted in Fig. 6(a), which ranges from 21.17 $\Omega\cdot cm^2$ (Al electrodes) to 8.62 $\Omega\cdot cm^2$ (Ni electrodes) at $V_G=0$ V and from 6.76 $\Omega\cdot cm^2$ (Al electrodes) to 0.07 $\Omega\cdot cm^2$ (Ni electrodes) at $V_G=10$ V gate bias. Hence, the ρ_C of Ni/ITZO contact is reduced by more than two time, and about two order of magnitude in comparison with that measured of Al/ITZO contact at $V_G=0$ V, and 10 V, respectively. From Fig. 6(b), the Φ of ITZO, Al, ITO, and Ni are 5.00–6.10 eV [9], 4.26 eV [12], 4.80 eV [16], and 5.04 eV [12], respectively. The activation energy and band gap of ITZO were 0.88 eV and 3.3 eV, respectively, which is consistent with our previous report [18]. For the AlO_x, the band gap from 6.66 to 9 eV was determined [19–21]. The result shows that the specific contact resistance decreases with the increase in the work function of the S/D metal electrodes. This also indicates that the work function of ITZO is higher than that of Ni electrodes, and in the range from 5.05 to 6.10 eV.

The negative shift of V_{TH} in Al/ITZO case can be explained by the increase of carrier concentration in the ITZO region after interfacial reaction. In addition, the enthalpies of formation for nickel oxide NiO ($\Delta H_{NiO}=-239.7$ kJ/mol), and Ni_2O_3 ($\Delta H_{Ni_2O_3}=-489.5$ kJ/mol) are almost similar to those of active layer composition. However, Ni only react with oxygen to give NiO_y at the temperature over 400 °C [22]. Hence, it is very difficult to form NiO_y at the ITZO/electrodes contact region. Although the carrier concentration at the interfacial region of Al/ITZO contact is higher than that of Ni/ITZO contact, the more difficult in the electron transportation lead to increasing the specific contact resistance and, therefore, reducing the ON current in the Al/ITZO TFT device.

It is found that the slope of ITO/ITZO TFT is larger than that of other electrodes. A possible explanation for this is

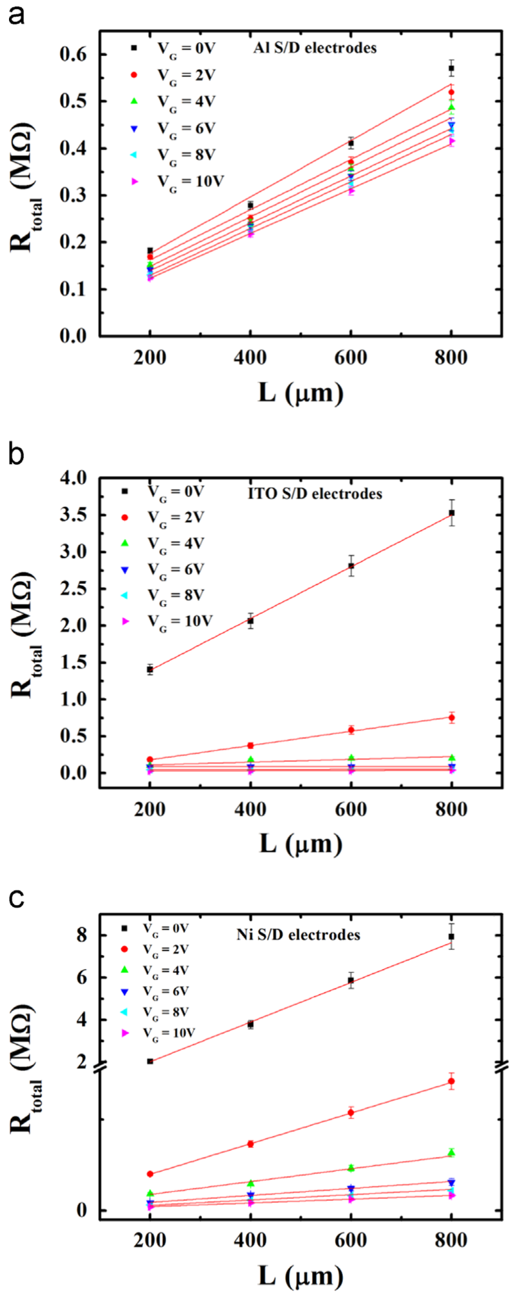

Fig. 5. Total resistance (R_{Total}) vs. electrode spacing plotted for V_G ranging from 0 to 10 V in 2 V steps.

the energy of absorbing ions to form the ITO film using sputtering method is higher than that of evaporation system. So the ITZO surface is damaged due to ion bombardment or UV generated by plasma [23], and then creates defect states at the ITO/ITZO interface. So the performance of the ITO/ITZO TFT device is degraded. In addition, further experiment is needed to confirm this conclusion.

Moreover, the positive gate voltage leads to an increase in the carrier density both in the channel and in the material beneath the contacts which decreases the

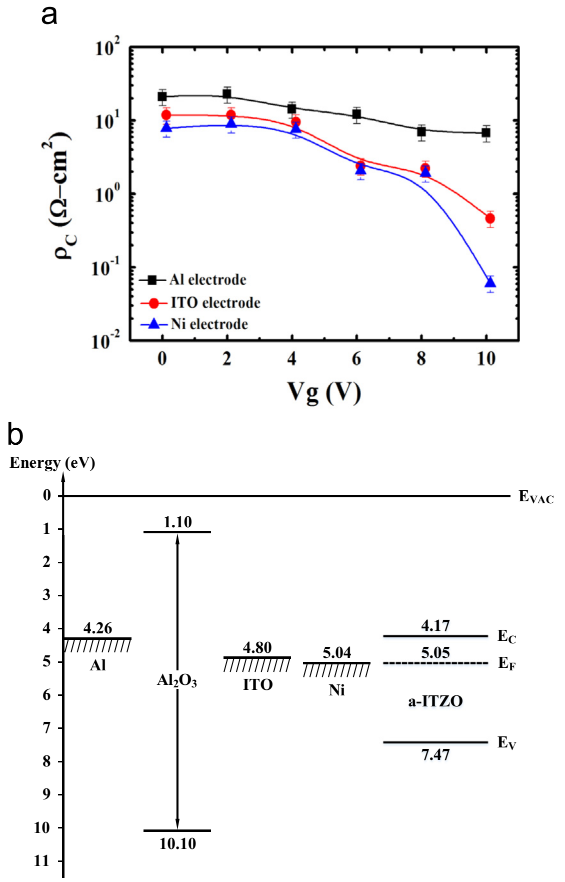

Fig. 6. (a) Specific contact resistance (ρ_C) between channel ITZO and metallization, and (b) schematic band diagram for ITZO TFT with Al, ITO, and Ni electrodes.

potential barrier to electron flow at the metallization/channel interface and increases the conductivity of the underlying channel material. Therefore, ρ_C decreases as the gate voltage increases.

4. Conclusion

The electrode effect on transistor characteristics is discussed in terms of contact resistance using a TLM method. The formation of high resistivity layer AlO_x at the interfacial region between Al and ITZO channel layer is one of the key components to affect the TFT performance. The reduction of channel length is consistent with the rapidly increasing of tunneling carrier through the AlO_x thin layer. Hence the V_{TH} shift to negative side due to the increase of carrier concentration in the ITZO active region. For the all S/D electrodes, the ohmic contacts are observed due to the linear *I–V* characteristics. The TFT devices using Ni S/D electrodes show the highest field effect mobility (16.09 $cm^2/V\cdot s$), improving the TFT ON/OFF current ratio (3.27×10^6) and sub-threshold slope (0.10 V · dec). The Al contacts show the largest ρ_C (from 21.17 to 6.76 $\Omega \cdot cm^2$ as the V_G from 0 to 10 V, respectively) which may be due to the formation of AlO_x at the Al/ITZO interface.

Acknowledgment

This research was supported by Basic Science Research Program through the National Research Foundation of Korea (NRF) funded by the Ministry of Science, ICT & Future 10 Planning (NRF-2014R1A1A3053287) and this work was also supported by Basic Science Research Program through the National Research Foundation of Korea (NRF) funded by the Ministry of Education (NRF-2010-0020210).

References

[1] T. Kamiya, H. Hosono, NPG Asia Mater. 2 (2010) 15–22.
[2] K. Nomura, H. Ohta, A. Takagi, T. Kamiya, M. Hirano, H. Hosono, Nature 432 (2004) 488–492.
[3] H. Hosono, J. Non-Cryst. Solids 352 (2006) 851–858.
[4] C.W. Ow-Yang, H.-y. Yeom, D.C. Paine, Thin Solid Films 516 (2008) 3105–3111.
[5] K.J. Saji, M.K. Jayaraj, K. Nomura, T. Kamiya, H. Hosono, J. Electrochem. Soc. 155 (2008) H390–H395.
[6] M. Grover, P. Hersh, H. Chiang, E. Kettenring, J. Wager, D. Keszler, J. Phys. D: Appl. Phys. 40 (2007) 1335.
[7] J.-Y. Noh, H. Kim, H.-H. Nahm, Y.-S. Kim, D.H. Kim, B.-D. Ahn, et al., J. Appl. Phys. 113 (2013) 183706.
[8] S. Lee, H. Park, D.C. Paine, Thin Solid Films 520 (2011) 3769–3773.
[9] C.A. Hoel, T.O. Mason, J.-F. Gaillard, K.R. Poeppelmeier, Chem. Mater. 22 (2010) 3569–3579.
[10] S. Lee, H. Park, D.C. Paine, J. Appl. Phys. 109 (2011) 063702–6.
[11] N.V. Duy, K. Baek, D.N. Son, W. Lee, K. Kim, B. Choi, et al., Jpn. J. Appl. Phys. 50 (2011) 4101.
[12] D.R. Lide, CRC Handbook of Chemistry and Physics, CRC Press, Boca Raton, FL, 2005 Internet Version, 2005, 〈http://www.hbcpnetbase.com〉.
[13] K.-H. Choi, H.-K. Kim, Appl. Phys. Lett. 102 (2013) 052103.
[14] T.T. Trinh, K. Jang, V.A. Dao, J. Yi, J. Appl. Phys. 116 (2014) 214504.
[15] D.H. Kang, J.U. Han, M. Mativenga, S.H. Ha, J. Jang, Appl. Phys. Lett. 102 (2013) 083508.
[16] Y. Shimura, K. Nomura, H. Yanagi, T. Kamiya, M. Hirano, H. Hosono, Thin Solid Films 516 (2008) 5899–5902.
[17] W.-S. Kim, Y.-K. Moon, K.-T. Kim, J.-H. Lee, B.-d. Ahn, J.-W. Park, Thin Solid Films 518 (2010) 6357–6360.
[18] K. Jang, J. Raja, J. Kim, C. Park, Y.-J. Lee, J. Yang, et al., Semicond. Sci. Technol. 28 (2013) 085015.
[19] J. Peng, Q. Sun, Z. Zhai, J. Yuan, X. Huang, Z. Jin, et al., Nanotechnology 24 (2013) 484010.
[20] M. Usman, C. Henkel, A. Hallén, ECS J. Solid State Sci. Technol. 2 (2013) N3087–N3091.
[21] C.H. Ahn, K. Senthil, H.K. Cho, S.Y. Lee, Sci. Rep. 3 (2013).
[22] P. Patnaik, Handbook of Inorganic Chemicals, McGraw-Hill, New York, 2003.
[23] J.D. Plummer, M.D. Deal, P.B. Griffin, Silicon VLSI Technology: Fundamentals, Practice, and ModelingPearson Education, India, 2009.